Int. J. Electrochem. Sci., 11 **(2016)** 8418 – 8429, doi: 10.20964/2016.10.19

International Journal of
ELECTROCHEMICAL
SCIENCE
www.electrochemsci.org

Preparation of Activated Carbons from Sisal Fibers as Anode Materials for Lithium Ion Batteries

Rui Du[1,2], *Zhangfa Tong*[1], *Chun Wei*[1,2], *Aimiao Qin*[2,3,*]

[1] School of Chemistry and Chemical Engineering, Guangxi University, Nanning 530001，PR China
[2] Guangxi Scientific Experiment Center of Mining, Metallurgy and Environment, Key Laboratory of New Processing Technology for Nonferrous Metals and Materials, Ministry of Education, College of Materials Science and Engineering, Guilin University of Technology, Guilin 541004，PR China.
[3] Guangxi Experiment Center of Information Science, Guilin 541004，PR China.
[*]E-mail: 317881264@qq.com

Received: 2 July 2016 / *Accepted:* 11 August 2016 / *Published:* 6 September 2016

Activated carbons have been prepared by pyrolysis of sisal fibers at different temperatures and hydrothermal treatment after pyrolysis. The obtained sisal fiber activated carbons (SFACs) are subjected to X-ray powder diffraction (XRD), BET-surface area, SEM, Cyclic voltammetry, Charge-discharge studies and Electrochemical impedance spectroscopy studies. The structures of the SFACs have been changed with the increased pyrolysis temperature and the hydrothermal treatment. The SFACs pyrolyzed at 900°C with hydrothermal treatment have more micropores than others. The electrochemical tests show that the SFACs pyrolyzed at 900℃ with hydrothermal treatment offer an extraordinarily high initial capacity of 998mAhg^{-1} and the charge-transfer resistance of 90Ω. The work highlights the potential to utilize sisal fibers to produce anode materials for lithium ion batteries.

Keywords: Sisal fiber, activated carbon, pyrolysis, hydrothermal treatment, lithium ion battery

1. INTRODUCTION

With the increasing of environment concerns and the development of electronic devices, there is a growing demand for the lithium ion batteries with high energy density [1-5]. However, the graphitic carbon which is widely used for the anode materials only have a theoretical specific capacity of 372 mAhg^{-1}, which can not meet the demands of high specific capacity lithium ion batteries [6-8]. So it is necessary to develop green and high specific capacity anode materials for lithium ion batteries.

Biomasses contain a large amount of carbon. We can prepare carbons by pyrolysis of biomasses at low temperature and with the protection of inert gas. Sometimes physical or chemical

activation is necessary for improving their properties. Amorphous carbons obtained from biomass such as coconut shell [9], rice husk [10], okara [11], and cocoon [12] have been reported.

Sisal is the characteristic plant in Guangxi, China. Sisal fiber is a major by-product in sisal industry. Sisal fibers have excellent mechanical property which are mainly used as textiles, artware and reinforced material [13]. In this article, we use sisal fibers for preparation of activated carbons, we call it SFACs. And we use the SFACs for anode materials of lithium ion batteries. Fig.1 shows the sisal and the sisal fibers.

The main objectives of our work are: (1) to develop a procedure for preparing the SFACs from sisal fibers by pyrolysis and hydrothermal treatment after pyrolysis. (2) to discuss the relations between the process of preparation and the structures of SFACs. (3) to determine the optimal conditions for preparing the SFACs with better electrochemistry performance for anode of lithium ion batteries.

Figure 1. Images of the sisal (A) and the sisal fibers (B).

2. EXPERIMENTAL

2.1 Preparation of materials

Sisal fibers were supplied by Guangxi sisal group Co. LTD. Sisal fibers were thoroughly washed with distilled water for several times. The washed sisal fibers were dried at 80°C in an oven for 8h and then the dried sisal fibers were placed in a tube furnace under a flow of N_2 gas at a rate of 3℃min^{-1} to reach pyrolysis temperature (700℃,800℃,900℃,1000℃,1100℃,1200℃) for a hold period of 1h. After cooling to room temperature naturally, we obtained the black carbonized products. The obtained carbons were ground in a mill, washed with distilled water, and dried at 60℃ for 12h. And then the carbons were activated with a hydrothermal method at 140 °C for 6 h. So we got 6 carbon samples by pyrolysis and 6 carbon samples by pyrolysis and hydrothermal method.

2.2 Characterization of materials

XRD was performed on a Panalytical X'Pert PRO diffractometer with nickel-filtered Cu Kα radiation and the scattering angles (2θ) from 10° to 70° in a step of 0.05°. The morphologies of the samples were examined by an Oxford S-4800 SEM. BET surface area measurements were carried out by Quantachrome NOVA 1200e surface area analyzer.

Electrochemical property were tested using coin cells (CR2025, half cell) with Li foil as counter electrode. Carbon electrodes electrochemical studies were prepared by blade-coating a slurry of 90 wt.% of the carbon fibers, 8 wt.% of polyvinylidene fluoride and 2 wt.% of acetylene black dispersed dispersed in N-methyl-2-pyrrolidinonesolvent on a copper foil and dried in a vacuum oven at 110 ℃ for 12 h. The cells were assembled in an argon-filled glove box (VACMO40-1). The electrolyte was 1 M LiPF6 dissolved in a mixture of ethylene carbonate, dimethyl carbonate and diethyl carbonate with a volume ratio of 1:1:1, and a Celgard 2400 microporous polypropylene film was used as separator.

The cyclic voltammogram (CV) and electrochemical impedance spectroscopy (EIS) measurements were carried out on an electrochemical working station (CHI660D, Shanghai, China) at room temperature. The CV measurements were tested between 0.7-3.3V. The EIS measurements were analyzed in the range of 100 kHz to 10mHz with alternating current (ac) amplitude of 0.5mV/s. The galvanostatic charge/discharge profiles were recorded at the voltage between 0.02 and 3.00 V at a rate of 0.1 C on a Neware BTS-5V10mA battery tester.

3. RESULTS AND DISCUSSION

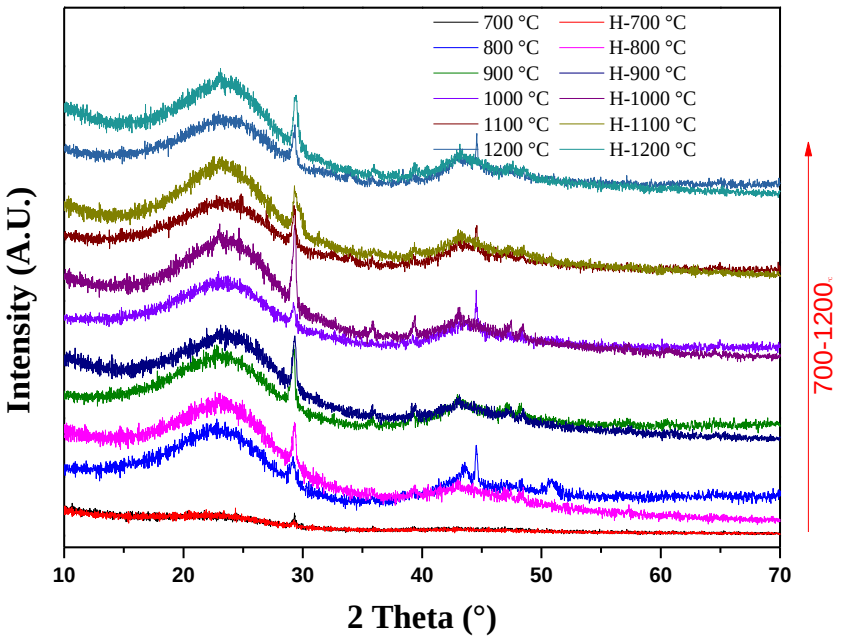

Figure 2. XRD of the SFACs obtained at 700-1200 ℃and hydrothermal treatment after pyrolysis.

Fig. 2 shows the XRD patterns of the SFACs obtained at 700-1200℃ without and with hydrothermal treatment. There are the peaks around 23° and 43° which indicate the SFACs have disordered structures [14, 15]. The peaks around 23° indicate parallel stacking of the carbon layers. Moreover, the peaks around 23° increase with the hydrothermal treatment at the same temperature. The peaks around 43° are typicality of honeycomb structure which are formed by sp^2 hybridized carbons [16]. There are some impurity peaks around 30° and 45°, we think there are some inorganic substances in the carbons.

According to Liu et al [17], the quantity of single layers in carbon materials prepared by pyrolysis can be calculated from the peak-to-background ratio(R), where R refers to the ratio of the X-ray peak intensity to the background intensity. The value of R depends on the single layer fraction (Table 1). At the same temperature, the R decrease with the hydrothermal treatment, which indicate that the single layers become mobile and result in their parallel orientation with respect to one another. The SFACs with lower R, having more single layers, generally showed larger specific capacity [18].

Table 1. R of the SFAC prepared at different pyrolysis temperature (700-1200℃)

700℃	800℃	900℃	1000℃	1100℃	1200℃
R（untreated） 1.89	2.28	2.20	2.39	2.43	2.44
R(hydrothermal)1.89	1.95	1.96	2.25	2.27	2.28

Table 2 summarizes the BET specific surface area, pore volume, density functional theory pore size and the specific capacity of SFACs prepared at different temperature (700-1200℃) without and with hydrothermal treatment. It is evident that the hydrothermal treatment greatly influences the BET surface area, pore volume , density functional theory pore size and specific capacity of SFACs at the same temperature. The SFACs prepared at 1200℃ with hydrothermal treatment show the highest BET surface area and pore size. The SFACs prepared at 900℃ with hydrothermal treatment show the highest specific capacity, It generally have the lower pore volume and the lower pore size which is more useful for lithium ion intercalation in the charge-discharge. So we conclude that the specific capacity of the SFACs is mainly decided by pore volume and pore size. These pore structures are the combination of micropores and mesopores [19], but the micropores can significantly influence the electrochemical performance of the SFACs.

Adsorption isotherms of N_2 at 77K on the SFACs obtained at 700-1200℃ without and with hydrothermal treatment are shown in Fig.3 and Fig.4. The shapes of isotherms change with the temperature and the hydrothermal treatment. The results indicate that the increase of temperature and the hydrothermal treatment greatly enhanced the pores development. It is generally that the volume absorbed increase with the increase of temperature and the hydrothermal treatment. According to the IUPAC classification, all the SFACs exhibit type I isotherm curves [20], the major nitrogen adsorption occurs at relative pressures less than 0.1. Relatively horizontal adsorption plateau appears at higher p/p0 values, which indicates that the micropores are dominant.

Table 2. BET-surface area measurements and the specific capacitances of SFACs prepared at different temperature without and with hydrothermal treatment.

Samples	BET Surface area (m^2g^{-1})	Pore volume (cm^3g^{-1})	Density functional theory pore size(nm)	Specific capacity ($mAhg^{-1}$)
700℃	3	0.011	1.410	16
800℃	11	0.024	1.410	567
900℃	12	0.019	1.126	630
1000℃	15	0.020	1.076	443
1100℃	99	0.070	1.126	400
1200℃	41	0.034	1.029	290
H-700℃	18	0.039	1.076	24
H-800℃	200	0.147	1.076	740
H-900℃	315	0.472	0.852	998
H-1000℃	370	0.377	1.029	601
H-1100℃	959	1.178	1.410	540
H-1200℃	1141	0.903	1.410	340

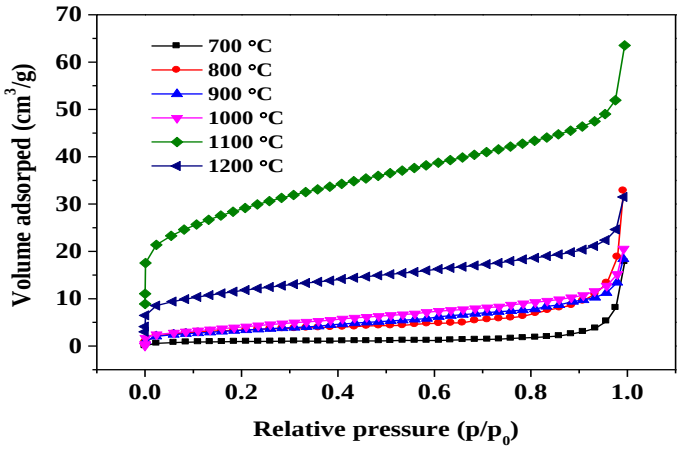

Figure 3. N_2 adsorption isotherms of the SFACs obtained at 700-1200℃ without hydrothermal treatment after pyrolysis.

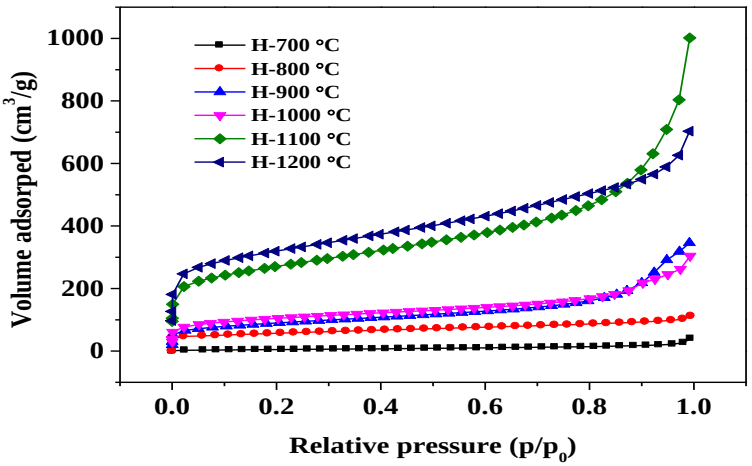

Figure 4. N_2 adsorption isotherms of the SFACs obtained at 700-1200℃ with hydrothermal treatment after pyrolysis.

The pore size distributions of the SFACs obtained at 700-1200℃without and with hydrothermal treatment are presented in Fig.5 and Fig.6, respectively. At the same temperature, the amount of pores in different regions changed markedly by the hydrothermal treatment, it is obvious that the SFACs obtained at 900℃ with hydrothermal treatment possess more micropores than others, which allow easier penetration of electrolytes and easier diffusion of lithium ions [21]. Therefore, both the hydrothermal treatment and the temperature are important factors to influence the pore structure of the SFACs, which is believed to affect the electrochemical performance.

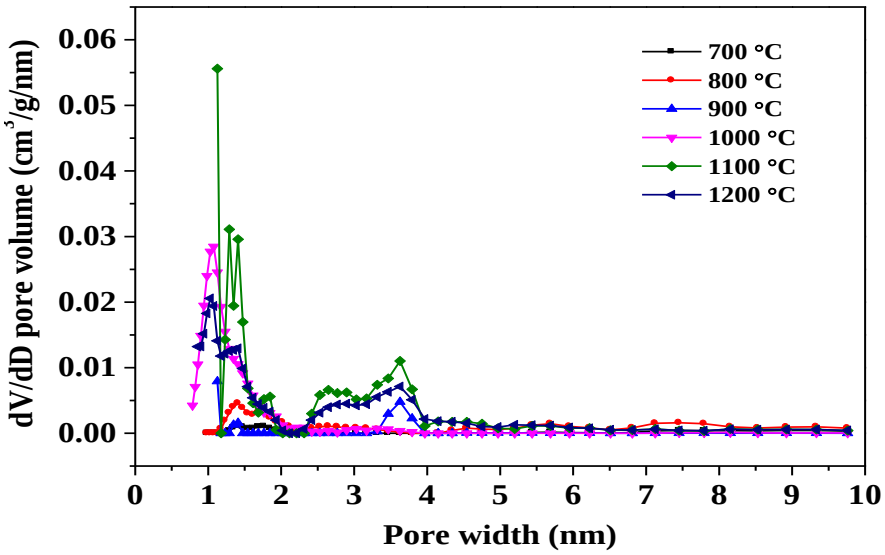

Figure 5. Pore size distribution of the SFACs obtained at 700-1200℃ without hydrothermal treatment after pyrolysis.

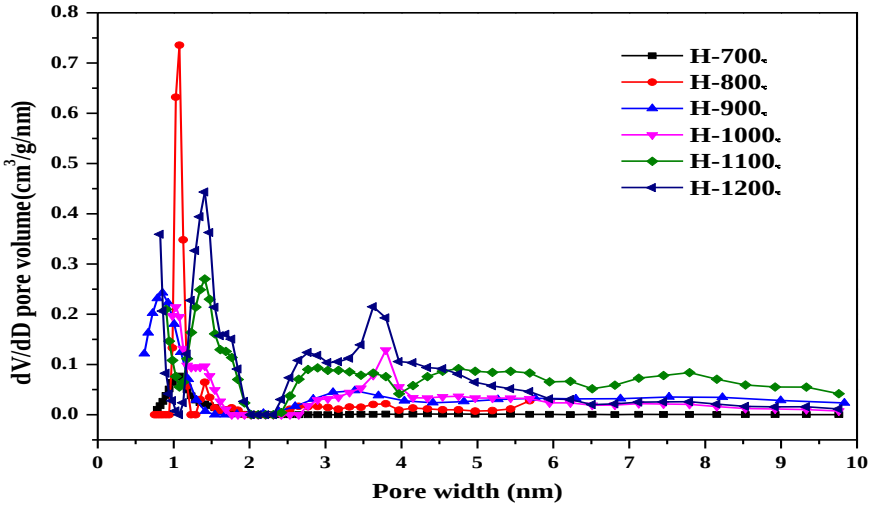

Figure 6. Pore size distribution of the SFACs obtained at 700-1200℃ with hydrothermal treatment after pyrolysis.

Fig. 7 (A-L) depicts the SEM images of the SFACs obtained at different temperatures (700-1200℃) without and with hydrothermal treatment. The SFACs have no definite shape for all samples. It can be seen that different surface morphology are observed for SFACs we prepared. It is generally that the particles of the SFACs with hydrothermal treatment are much smaller than the untreated, and the surface of the SFACs with hydrothermal treatment is rougher than the untreated. By further observation of the enlarged images of the SFACs, more nanopores can be found for the SFACs with hydrothermal treatment. And whether the hydrothermal treatment or not, the pores looks more clearly with the increase of temperature. According to the table2, the H-900℃ SFACs have the smallest pore size(0.852nm), it shows the highest specific capacity(998 mAhg-1). From Fig.7F, there are more layered structure with micropores on the H-900℃ SFACs than the others. These micropores have lots of locations for lithium storage [22], which can effectively enhance the penetrability of electrolytes into the interior surfaces and provide short and low-resistant ion diffusion channels to facilitate ion transportation [21], that improve the electrochemical performance significantly. So we conclude the pore size (micropore) may be dominant to specific capacitance of the SFACs.

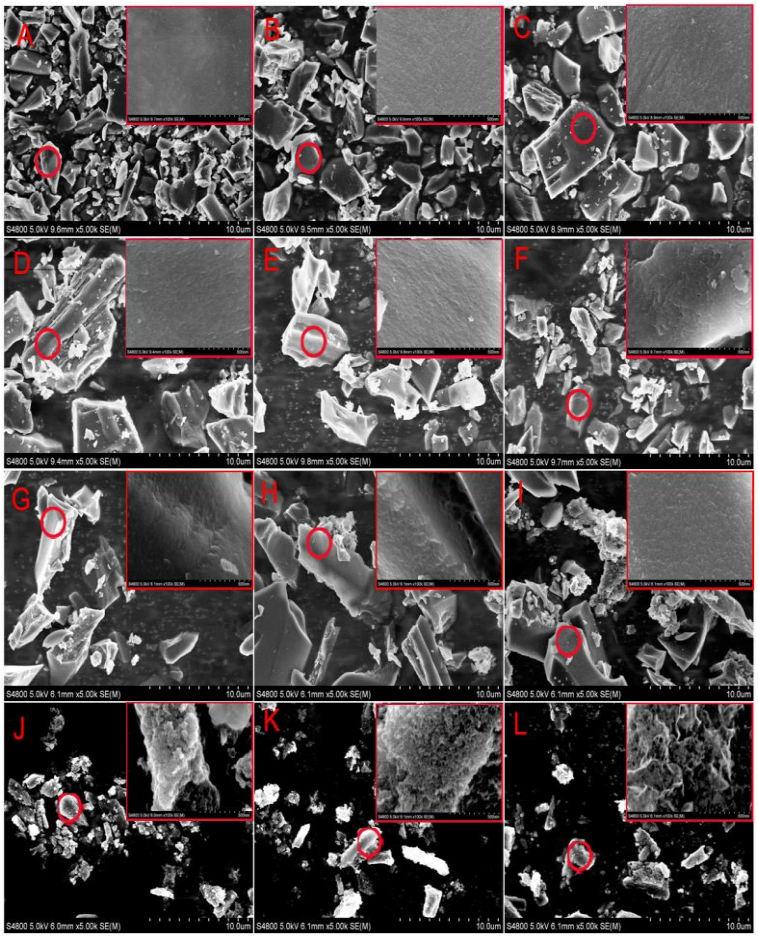

Figure 7. SEM of the SFACs obtained at 700-1200℃ with and without hydrothermal treatment after pyrolysis (ABC, 700-900℃, untreatment; DEF, 700-900℃, hydrothermal treatment; GHI, 1000-1200℃, untreatment; JKL, 1000-1200℃, hydrothermal treatment).

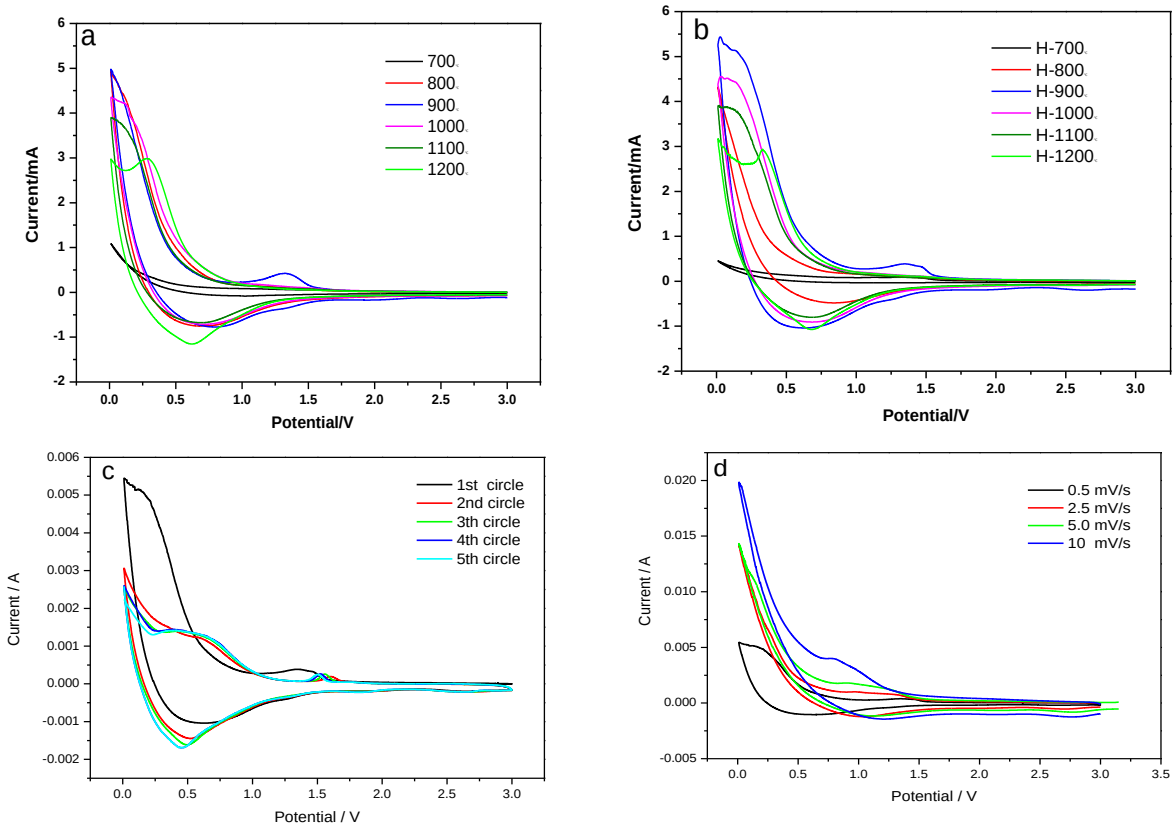

Figure 8. The first CV cycle of the SFACs obtained at 700-1200℃ with(b)and without(a)hydrothermal treatment at scan rate of 0.5mV/s; The first five CV cycles of the SFACs obtained at 900℃ with hydrothermal treatment scan rate of 0.5mV/s (c); The first CV cycles of the SFACs obtained at 900℃ with hydrothermal treatment at different scan rates of 0.5, 2.5 , 5.0, 10mV/s(d).

The first CV circle of the SFACs obtained at 700-1200℃ without and with hydrothermal treatment at scan rate of 0.5mV/s are shown in Fig. 8a-b. It can be seen in Fig. 8a-b that the CV of the SFACs obtained at 900℃ without and with hydrothermal present better electrochemical character than others. There is a pair of peaks on curves between 0.5 and 1.5V. These are attributed to the presence of a redox couple in this potential region. The H-900℃ exhibits the largest area of loop, suggesting the highest capacity, which is same to the table 2. So it concluded that the pyrolysis of 900℃ with hydrothermal treatment is the most suitable in our preparation. The Fig. 8c is the first five CV cycles of the SFACs obtained at 900℃ with hydrothermal treatment at scan rate of 0.5mV/s. The current in the first cycle below 0.5V is obviously larger than that of the others. The extra current in the first cycle could be ascribed to the electrolyte which is irreversibly reduced at low-voltage to form a solid electrolyte interphase (SEI) layer [23-26]. The peak around 1.5V decrease after the first cycle, and the areas of the cycles tend to be similar to each other, implying the stability of the SEI layer and the structure of the SFACs [27]. The Fig. 8d is the CV cycles of the SFACs obtained at 900℃ with hydrothermal treatment at different scan rates of 0.5,2.5,5,10mV/s. It could be seen from Fig.8d that the peaks around 1.5V disappear on the cycles at scan rates of 2.5,5.0,10mV/s. With the increase of scan rate, the cycles become more deformedly. It is indicated that the electrolytes had enough time to

enter into micropores for small scan rate, and the micropores were effectively used for forming SEI layer [28].

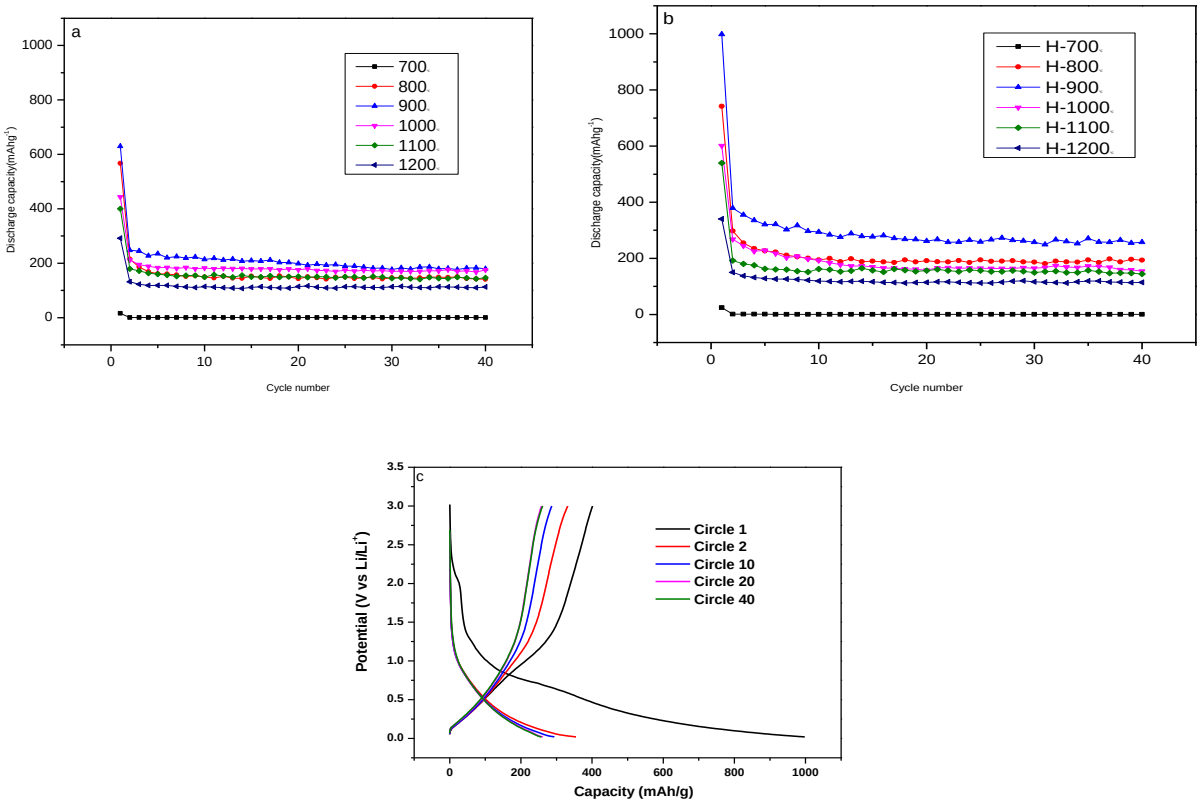

Figure 9. Cycling performance of the SFACs obtained at 700-1200℃ with(b) and without(a) hydrothermal treatment; The charge /discharge curves of the electrode based on the SFACs obtained at 900℃ with hydrothermal treatment after pyrolysis(c).

Fig. 9 show the cycling performance of SFACs obtained at different temperature without (a) and with(b) hydrothermal treatment. It is quite obvious from the figure that the SFACs obtained at 900℃ with and without hydrothermal treatment have the highest discharge capacitance than that of other samples. At lower temperature(700/800℃), there is not enough thermal energy for some graphene sheets to rotate into a parallel alignment [27], which results in a part of non-parallel and unorganized single layers in SFACs [29]; At higher temperature(1000/1100/1200℃), the thermal energies reach values extra high to make the mesopores collapse and fuse into macropores, which leads to a decrease for the locations of lithium insertion [30,31]. And there are the capacity fade of all SFACs, which means that a significant part of the lithium is unavailable for reversible reaction, rendering a significant parts of the activated material deadweight. The first discharge capacity(998mAhg^{-1}) of the SFACs obtained at 900℃ with hydrothermal treatment is largely higher than the SFACs(630 mAhg^{-1}) obtained at 900℃ without hydrothermal treatment. From the Table 2 and the Fig.5-7, we can find that the structure of the SFACs is greatly changed by hydrothermal treatment. Fig.9c shows the discharge/charge curves of the electrode based on the SFACs obtained at 900℃ with

hydrothermal treatment. During the first charge and discharge, there is the formation of SEI layer which prevents the electrolyte from undergoing decomposition on the SFACs; after the initial charge and discharge, the capacity of the SFACs becomes gradually stable.

To further study the electrochemical performance of the SFACs, the EIS plots for the before discharged SFACs electrodes obtained at different temperature without and with hydrothermal treatment are shown in Fig.10. The high frequency intercept on the real axis represents the ohmic resistance, which includes the electrolyte resistance and the electrode resistance. The semicircle at high-middle frequency is attributed to the charge-transfer resistance. The inclined line at the low-frequency region refers to the ion diffusion within the electrode. The smaller the diameter of semicircle is, the lower the charge-transfer resistance of an electrode. It can be easily observed that the charge-transfer resistance of the 900℃ and the H-900℃ cathode are obviously lower than that of the others. And the charge-transfer resistance of the H-900℃ is 90Ω,which is lower than 130Ω of the 900℃. We think the hydrothermal treatment makes some organic substances of the SFACs decomposed, so the charge-transfer resistance decreased, and the capacitance of the SFACs has been improved.

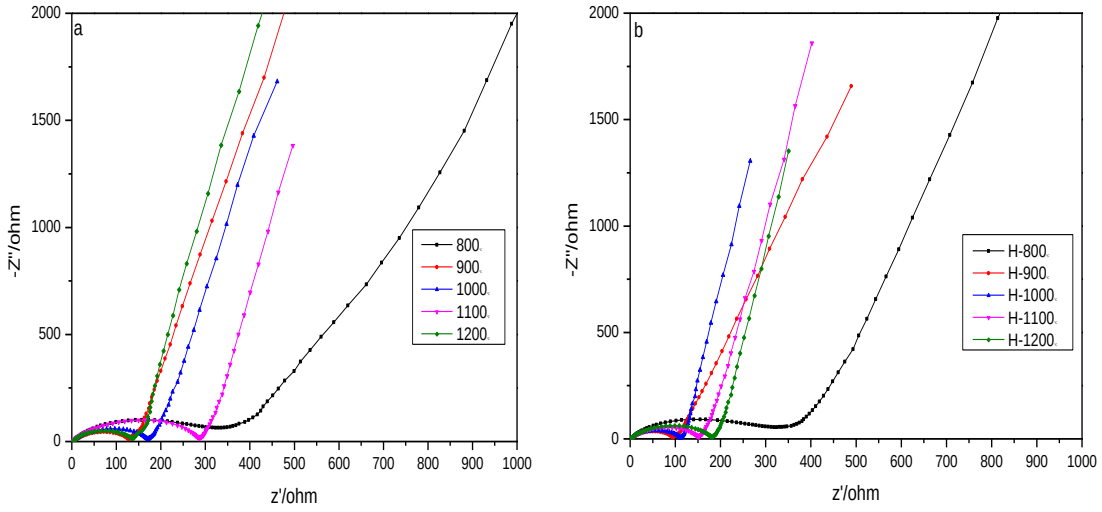

Figure 10. Nyquist plots of the electrochemical Impedance of before discharged SFACs electrodes obtained at 700-1200℃with(b) and without(a) hydrothermal treatment.

4. CONCLUSIONS

We have synthesized the sisal fiber activated carbons (SFACs) from the sisal fiber by pyrolysis and hydrothermal treatment. According to the materials characterizations and electrochemical characterizations, we find the suitable preparation conditions are pyrolysis at 900℃ and hydrothermal treatment after pyrolysis for the anode materials of lithium ion batteries. The SFACs show unique structural features with rich micropores which offer lots of locations for lithium storage, and it obviously improve the electrochemical performance. The initial capacity of the SFACs is 998mAhg^{-1} and its charge-transfer resistance is 90Ω. Although there are the capacity fade after the first charge-discharge, the capacity of the SFACs become gradually stable. In future study, we will try to increase

the capacity and decrease the capacity fade for improving the reversibility capacity of the SFACs. We believe the sisal fiber activated carbons will be the promising anode materials for lithium ion battery.

ACKNOWLEDGEMENTS
This work was financially supported by the NSFC (51564009, 51468011 and 51463007), the NSF of Guangxi Province (2015GXNSFDA139035, 2014GXNSFAA118331, and 2014GXNSFDA118006)

References

1. M. Z. Jacobson, *Energy & Environmental Science*. 2 (2009) 148.
2. M. Armand, J. M. Tarascon, *Nature.* 451 (2008) 652.
3. A. Manthiram, *Journal of Physical Chemistry Letters*. 2 (2011) 176.
4. O. K. Park, Y. Cho, S. Lee, H.C. Yoo, H.K. Song, J. Cho, *Energy & Environmental Science*. 4 (2011) 1621.
5. J. B. Goodenough, Y. Kim, *Chemistry of Materials*. 22 (2010) 587.
6. L. Ji, Z. Lin, M. Alcoutlabi, X. Zhang, *Energy & Environmental Science*. 4 (2011) 2682.
7. J. R. Dahn, T. Zheng, Y. H. Liu, J. S. Xu, *Science*. 270 (1995) 590.
8. S. Yata, H. Kinoshita, M. Komori, N. Ando, T. Kashiwamura, T. Harada, K. Tanaka, T. Yamabe, *Synthetic Metals*. 62 (1994) 153.
9. Y. J. Hwang, S. Jeong, J. Shin, K. S. Nahm, A. M. Stephan, *Journal of Alloys and Compounds*. 448 (2008) 141.
10. GT. K. Fey, C. -L. Chen, *Journal of Power Sources*. 97 (2001) 47.
11. T. Zhou, H. Wang, S. Ji, H. Feng, R. Wang, *Fuel Cells*.14 (2014) 296.
12. H. Yang, H. Wang, S. Ji, Y. Ma, V. Linkov, R. Wang, *Journal of Solid State Electrochemistry*. 18 (2014) 1503.
13. Y. Li, Y. W. Mai, L. Ye, *Composites Science and Technology*. 60 (2000) 2037.
14. J.R. Dahn, A.K. Sleigh, H. Shi, J.N. Reimers, Q. Zhong, B. M. Way, *Electrochimica Acta*. 38 (1993) 1179.
15. G. Q. Wang, D. L. Wang, S. Kuang, *Renewable Energy*. 63 (2014) 708.
16. M. Stephan, T. P. Kumar, R. Ramesh, *Materials Science and Engineering*: A. 430 (2006) 132.
17. Y. Liu, J. S. Xue, T. Zheng, J. R. Dahn, *Carbon*. 34 (1996) 193.
18. W. Xing, J. Xue, T. Zheng, A. Gibaud, J. Dahn, *Journal of the Electrochemical Society*. 143 (1996) 3482.
19. T. Morishita, Y. Soneda, T. Tsumura, M. Inagaki, *Carbon*. 44 (2006) 2360.
20. M. S. El-Geundi, *Adsorption Science and Technology*. 15 (1997) 777.
21. D. W. Wang, F. Li, M. Liu, G. Q. Lu, H. M. Cheng, *Angewandte Chemie International edition*. 120 (2008) 379.
22. Y. P. Wu, C. R. Wan, C. Y. Jiang, S. B. Fang, Y. Y. Jiang, *Carbon.* 37 (1999) 1901.
23. H. Zhou, S. Zhu, M. Hibino, I. Honma, M. Ichihara, *Advanced Materials*. 15 (2003) 2107.
24. V. Subramanian, H. Zhu, B. Wei, *Journal of Physical Chemistry* B. 110 (2006) 7178.
25. Y. K. Choi, K. I. Chung, W. S. Kim, Y. E. Sung, *Microchemical Journal*. 68 (2001) 61.
26. J. S. Gnanaraj, M. D. Levi, E. Levi, G. Salitra, D. Aurbach, E. F. John, C. Agnes, *Journal of Electrochemical Society*. 148 (2001) A525.
27. Y. Li, F. Wang, J. Liang, et al, *New Journal of Chemistry*. 40 (2016) 325.
28. X. L. Li, C. L. Han, X.Y. CHEN, C. W. Shi, *Microporous and Mesoporous Materials*. 131 (2010) 303.
29. Y. J. Hwang, S. K. Jeong, K. S. Nahm, J. S. Shin, A. M. Stephan, *Journal of Physics and Chemistry of Solids.* 68 (2007) 182.

30. S. Han, D. Jung, J. Jeong, *Chemical Engineering Journal*. 254 (2014) 597.
31. G. T. K. Fey, D. C. Lee, Y. Y. Lin, *Synthetic Metals*. 139 (2003) 71.